

Jets and Prompt Photons in Photoproduction at ZEUS

L. E. Sinclair

for the ZEUS Collaboration

Abstract

In the ZEUS experiment at HERA, photoproduction processes have been studied for photon-proton centre-of-mass energies in the range $100 < W_{\gamma p} < 300$ GeV and jet transverse energies extending to $E_T^{\text{jet}} \sim 70$ GeV. The data contribute to our understanding of QCD dynamics, and also provide new constraints on the photon's parton density.

*talk given at the XXIX International Conference on High Energy Physics (ICHEP '98)
Vancouver, Canada. August, 1998.*

1 Introduction

There has been tremendous progress in the understanding of photon induced reactions since the start of HERA operation. Up to the end of 1994, HERA had delivered a total of 7 pb^{-1} of ep data. The analysis of this data was fruitful. ZEUS was able to clearly establish evidence for both the direct and the resolved classes of process. These are illustrated at leading order (LO) in Figure's 1(a) and (b).

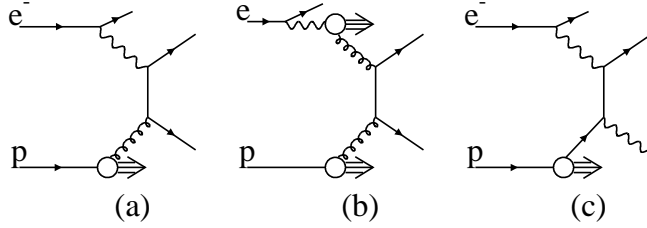


Figure 1: Examples of leading order diagrams for (a) direct photoproduction, (b) resolved photoproduction and (c) direct prompt photon photoproduction.

An observable quantity was defined which extended the distinction between direct and resolved processes to all orders of perturbation theory, $x_\gamma^{\text{OBS}} = \sum_{\text{jets}} E_T^{\text{jet}} e^{-\eta^{\text{jet}}} / 2E_\gamma$ where the sum runs over the two highest transverse energy jets in the final state. Direct processes contribute primarily at high x_γ^{OBS} and resolved processes contribute at low x_γ^{OBS} . However the comparison with theory has been hampered by the need to introduce models such as secondary interactions between the photon and proton constituents in order to understand the resolved processes at $E_T^{\text{jet}} \sim 6 \text{ GeV}$.

By the end of 1997 running HERA had delivered an order of magnitude more data, $\sim 70 \text{ pb}^{-1}$. This large data-set allows the exploration of photoproduction up to much higher jet transverse energies where a strong confrontation with the predictions of perturbative QCD (pQCD) may be made. This is illustrated in Figure 2 [1]. Here the x_γ^{OBS} distribution is shown for photoproduction events where at least two jets are produced, one with $E_T^{\text{jet}} > 14 \text{ GeV}$ and the other with $E_T^{\text{jet}} > 11 \text{ GeV}$ where the jet pseudorapidities satisfy $-1 < \eta^{\text{jet}} < 2$. The results are compared with the Monte Carlo predictions from HERWIG [2], which implements the leading order

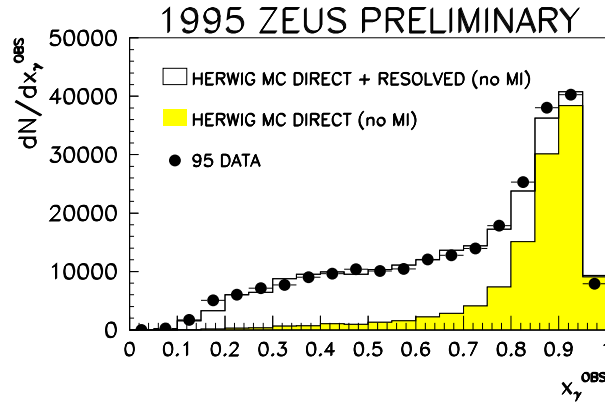


Figure 2: Distribution of x_γ^{OBS} . The black dots show the uncorrected data. The histogram shows the HERWIG prediction with the contribution due to LO direct processes shaded. Multiple interactions have not been included in the simulation.

matrix elements together with a parton shower. A good description of the data is provided by HERWIG across the entire x_γ^{OBS} range, without having to resort to additional parameters. This facilitates the interpretation of the data within pQCD.

This high accumulated luminosity also gives access to such infrequent processes as prompt photon production, illustrated in Figure 1(c), and multijet production. In this talk results are presented on four topics; single and dijet inclusive cross sections [1, 3], prompt photon production [4], the evolution of the photon's structure with virtuality [5] and two and three-jet angular distributions in high mass events [6, 7].

2 Single and Dijet Inclusive Cross sections

In hadron-hadron collisions, jets of final-state hadrons are commonly determined by cone algorithms which seek to maximize the transverse energy produced inside a cone of fixed radius in pseudorapidity and azimuth. However the confrontation of data and theory using such algorithms is compromised by the need to introduce an ad-hoc parameter R_{SEP} into the theory, in order to simulate merging effects [8]. A clustering algorithm which combines particles with small relative transverse momenta, k_T , into jets has been developed for use in hadron-hadron collisions [9, 10]. With this algorithm it is not necessary to introduce additional parameters in order to compare data and theory. In the results presented here the k_T clustering algorithm has been used.

Figure 3 presents the inclusive jet cross section, $d\sigma/dE_T^{\text{jet}}$, for jets with $-0.75 < \eta^{\text{jet}} < 2.5$ and for centre-of-mass (CM) energies in the range $134 < W_{\gamma p} < 277$ GeV [3]. The cross section falls by 4 orders of magnitude

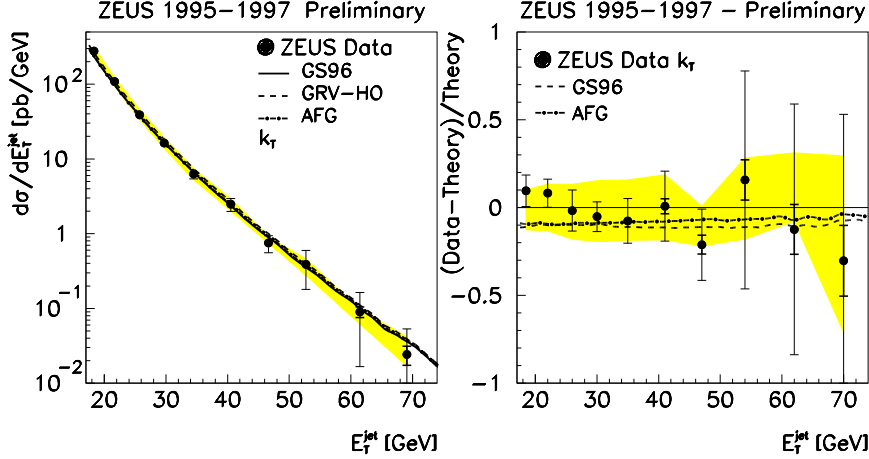


Figure 3: Left: Inclusive jet production cross section, $d\sigma/dE_T^{\text{JET}}$. Right: Fractional difference between the measured cross section and the pQCD prediction using the GRV HO parametrization of the photon parton densities. The dots show the data. The inner error bars show the statistical error. The outer error bars show the quadratic sum of the statistical and systematic uncertainties with the exception of the absolute energy scale uncertainty which is shown separately as a shaded band.

over the E_T^{jet} range, extending to ~ 70 GeV. This behaviour is impressively reproduced in the theory. The three curves show $\mathcal{O}(\alpha_s^2)$ pQCD calculations for different parametrizations of the parton densities of the photon. Within the current measurement uncertainties all are consistent with the data. This is more clear in the plot on the right which shows the relative difference with respect to the calculation using the GRV HO parametrization.

The dijet inclusive photoproduction cross section as a function of the pseudorapidity of one of the jets, $d\sigma/d\eta_2$, is shown in Figure 4, in three bins of the pseudorapidity of the other jet, η_1 [1]. Here the events have been required to have at least one jet with $E_T^{\text{jet}} > 14$ GeV and at least one other with $E_T^{\text{jet}} > 11$ GeV. The photon-proton CM energies have been limited to the range $212 < W_{\gamma p} < 277$ GeV, in order to enhance sensitivity to the photon's parton densities. Indeed, by comparison with the next-to-leading order (NLO) calculations we find that one parton density set (GRV) is favoured over another (GS96). It is worth emphasizing that GS96 is a modern set, consistent with the world data on F_2^γ . The ability of the data to disfavour this, indicates that ZEUS is contributing photoproduction information in a heretofore unexplored regime.

3 Prompt Photon Production

A clean laboratory for testing QCD predictions is provided by prompt photon production, Figure 1(c). An inclusive prompt photon measurement, tagging only the final-state hard photon, may be directly compared with pQCD calculations, with neither concern for jet definition matching between theory and experiment, nor for hadronization uncertainties.

In Figure 5 the inclusive prompt photon cross section with respect to the photon's pseudorapidity, $d\sigma/d\eta^\gamma$, is shown. The events lie in the range $120 < W_{\gamma p} < 270$ GeV and have at least one photon of transverse energy $5 < E_T^\gamma < 10$ GeV. The cross section is compared with predictions for two different parametrizations of the photon's structure, GRV and GS. Again we find that there is a preference for the GRV parton densities over the GS parton densities.

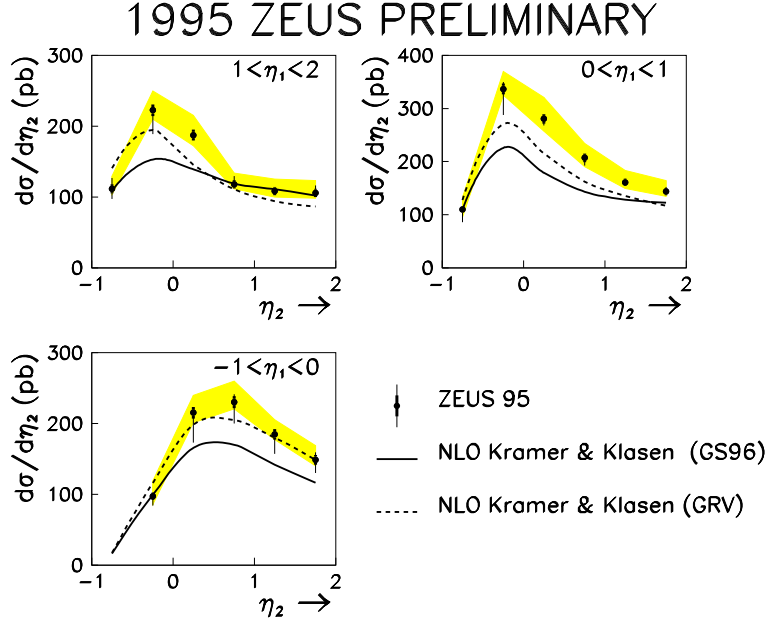


Figure 4: Dijet inclusive cross section, $d\sigma/d\eta_2^{\text{jet}}$. Error bars are as described for Figure 3. NLO calculations for two parametrizations of the photon parton distributions are shown by the solid and dashed curves.

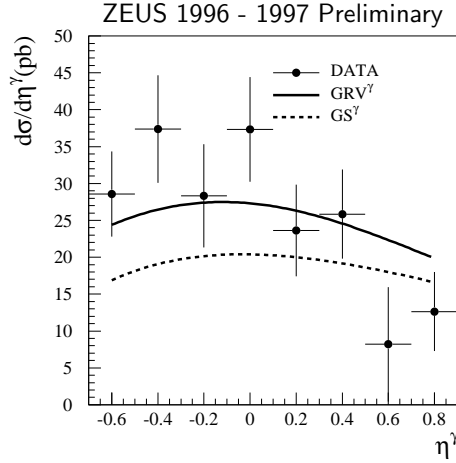


Figure 5: Inclusive prompt photon photoproduction cross section, $d\sigma/d\eta^\gamma$. The errors shown are statistical only. The lines show QCD NLO predictions for two different parametrizations of the photon parton densities. A systematic uncertainty of $\pm 15\%$ should be allowed.

4 Virtual Photon Structure

In addition to asking about the parton density of the real photon, one can ask how that structure will evolve with the negative invariant mass squared of the photon, or the photon's virtuality, Q^2 . One expects that as Q^2 increases, less time is available for the photon to develop a complicated hadronic structure.

In Figure 6, the uncorrected distribution of x_γ^{OBS} is shown for events with at least two jets of $E_T^{\text{jet}} > 6.5$ GeV and $-1.125 < \eta^{\text{jet}} < 1.875$, in three different ranges of Q^2 . These distributions indicate that the frequency of resolved processes (which populate low x_γ^{OBS}) decreases with respect to the frequency of direct processes, as Q^2 increases. To quantify this observation, the ratio of the dijet inclusive cross section for $x_\gamma^{\text{OBS}} < 0.75$ to the dijet inclusive cross section for $x_\gamma^{\text{OBS}} \geq 0.75$ has been measured as a function of Q^2 . This is also shown in Figure 6. This measurement confirms the expectation that resolved photoproduction processes are suppressed as the photon's virtuality increases.

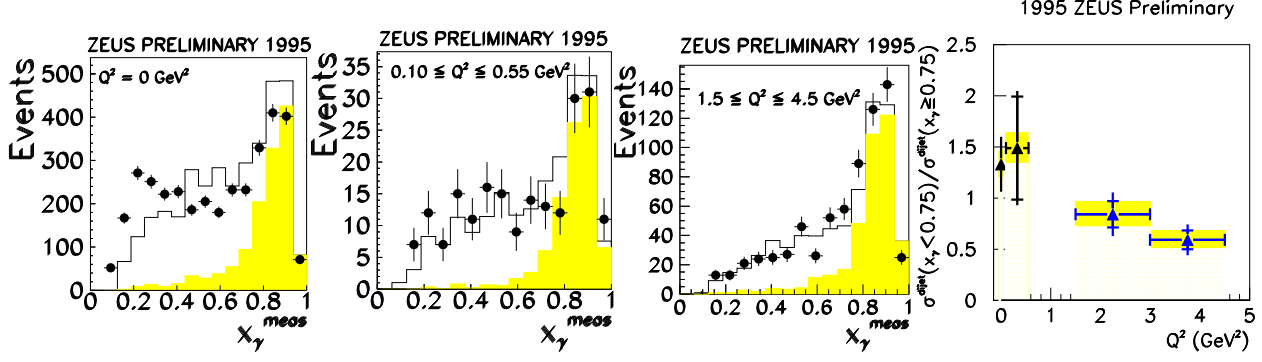


Figure 6: Uncorrected x_{γ}^{meas} (x_{γ}^{OBS}) distributions in three photon virtuality ranges where the error bars show the statistical errors only. The histogram shows the HERWIG prediction with the LO direct contribution shaded. Also, the ratio of the resolved to the direct dijet cross sections versus Q^2 where the error bars are as described for Figure 3.

5 High Mass Dijet and Three-jet Distributions

As well as probing the partons within the photon, the ZEUS photoproduction data can be used to learn something about the dynamics of parton-parton scattering. The definition of the scattering angles in two and three-jet events are illustrated in Figure 7.

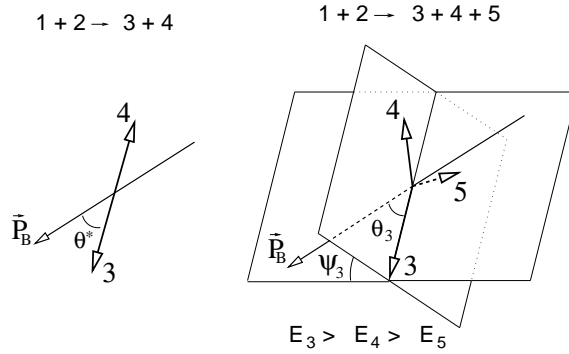


Figure 7: Centre-of-mass frame diagrams of two and three-body scattering angles. The beam direction is indicated by \vec{P}_B .

In Figure 8 the dijet invariant mass distribution is shown for events in which the scattering angle in the dijet rest frame, θ^* , satisfies $|\cos \theta^*| < 0.8$ [6]. Resonances decaying to two jets would be expected to show an

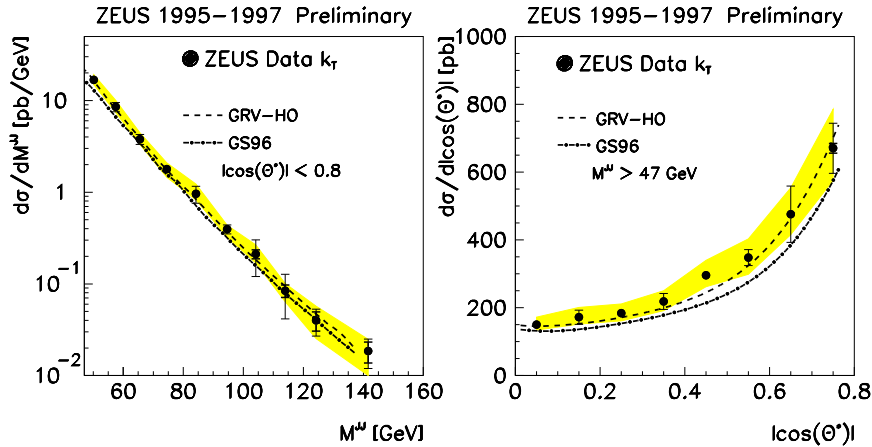


Figure 8: Left: Differential dijet cross section, $d\sigma/dM^{JJ}$. Right: Differential dijet cross section, $d\sigma/d|\cos \theta^*|$. The error bars are as described for Figure 3. NLO QCD calculations for two parametrizations of the photon parton distributions are shown by the dashed and dot-dashed lines.

excess above the pQCD predictions in a limited range of M^{JJ} . No evidence for this is seen.

The scattering angle in the dijet CM frame in photoproduction has been shown to be sensitive to the spin of the exchanged parton [11]. The $\cos\theta^*$ distribution is shown for the events with $M_{JJ} > 47$ GeV on the right in Figure 8. The NLO pQCD calculations are in good agreement with the data confirming that the dynamics of two-jet production are well understood.

ZEUS has also measured the high-mass three-jet cross section, $d\sigma/dM_{3J}$, as shown in Figure 9 [7]. The

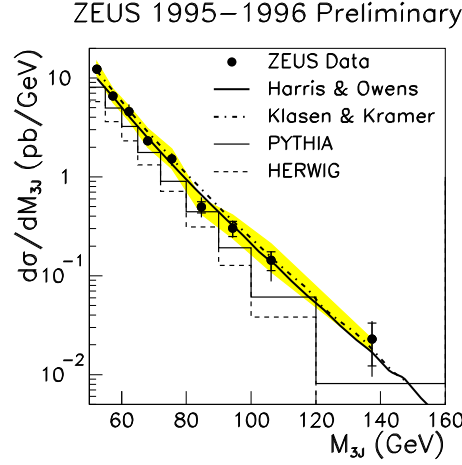


Figure 9: The three-jet cross section $d\sigma/dM_{3J}$. The error bars are as described for Figure 3. $\mathcal{O}(\alpha_s^2)$ pQCD calculations by two groups of authors are shown by thick solid and dot-dashed lines. The thin solid and dashed histograms show the predictions from PYTHIA and HERWIG.

$\mathcal{O}(\alpha_s^2)$ pQCD calculations from two groups of authors (Harris & Owens, Klasen & Kramer) provide a good description of the data, even though they are leading order for this process. Monte Carlo models also generate three-jet events through the parton shower mechanism and both PYTHIA [12] and HERWIG reproduce the shape of the M_{3J} distribution.

For three-jet events there are two relevant scattering angles as illustrated in Figure 7. The distributions of $\cos\theta_3$ and ψ_3 are shown in Figure 10. The $\cos\theta_3$ distribution resembles that of $\cos\theta^*$ and exhibits forward and

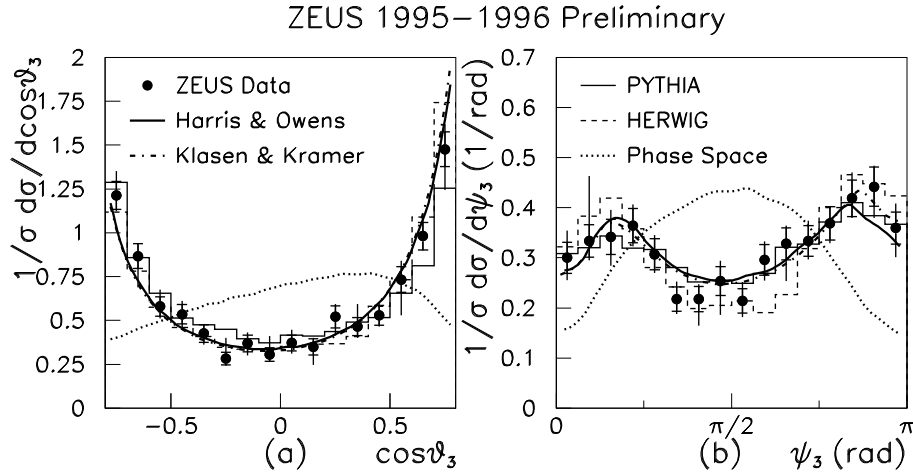


Figure 10: Distribution of the angles $\cos\theta_3$ and ψ_3 . The dotted curve shows the distribution for a constant matrix element. Other details are as described for Figure 9.

backward peaks. It is well described in both $\mathcal{O}(\alpha_s^2)$ pQCD calculations and parton shower models. The ψ_3 distribution is peaked near 0 and π indicating that the three-jet plane tends to lie near the plane containing the highest energy jet and the beam. This is particularly evident if one considers the ψ_3 distribution for three partons uniformly distributed in the available phase space. The phase space near $\psi_3 = 0$ and π has been depleted by the E_T^{jet} cuts and by the jet-finding algorithm. The pQCD calculations describe perfectly the ψ_3 distribution. It is remarkable that the parton shower models PYTHIA and HERWIG are also able to reproduce the ψ_3 distribution.

Within the parton-shower model it is possible to determine the contribution to three-jet production from initial-state radiation (ISR) and final-state radiation (FSR). In Figure 11 the cross section $d\sigma/d\psi_3$ is shown, along with the area-normalized ψ_3 distribution. Here the PYTHIA prediction is shown for FSR only, ISR only,

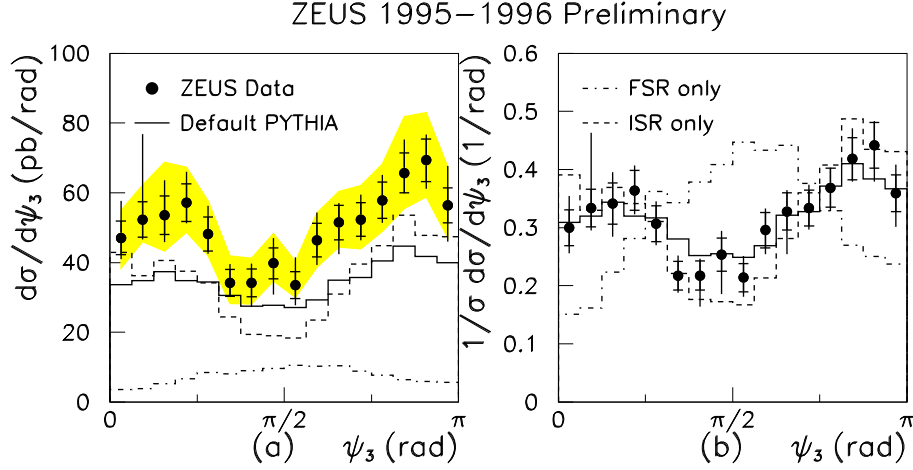


Figure 11: (a) The cross section $d\sigma/d\psi_3$ and (b) the normalized distribution of ψ_3 . The error bars are as described for Figure 3. The solid line shows the default PYTHIA prediction, the dashed line shows the prediction with FSR switched off and the dot-dashed line shows the distribution with ISR switched off.

and default PYTHIA which includes the interference of these two. Clearly, ISR is predominantly responsible for the three-jet production.

The QCD phenomenon of colour coherence may be expected to favour topologies in which the softest jet is radiated close to the plane containing the highest energy jet and the beam. Figure 12 shows $d\sigma/d\psi_3$ and $1/\sigma d\sigma/d\psi_3$ compared with the expectations from HERWIG, default PYTHIA, and PYTHIA with coherence

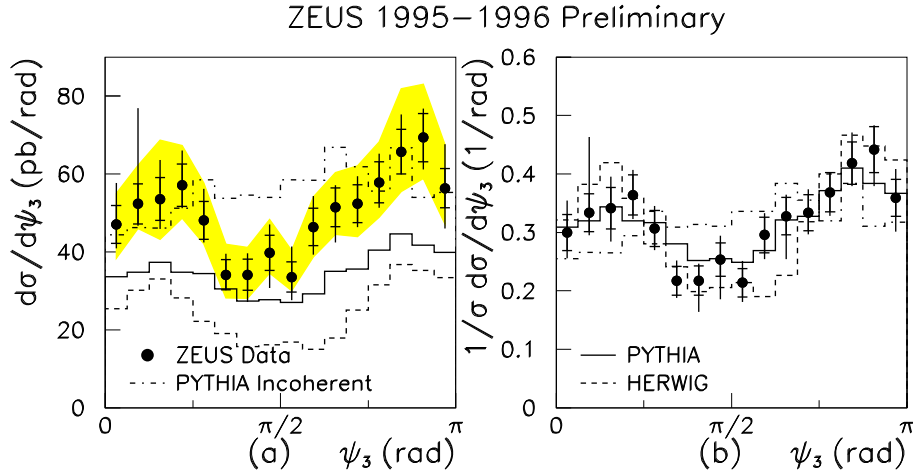


Figure 12: (a) The cross section $d\sigma/d\psi_3$ and (b) the normalized distribution of ψ_3 . The error bars are as described for Figure 3. The PYTHIA and HERWIG predictions are shown by the solid and dashed lines and the dashed-dotted line shows the PYTHIA prediction with colour coherence switched off.

switched off. Coherence suppresses large angle emissions leading to a depletion of the ψ_3 distribution near $\psi_3 = \pi/2$. The incoherent prediction is relatively flat. Coherence in the parton shower is required by the data. However the current measurement precision is insufficient to discriminate between the two models, HERWIG and PYTHIA.

6 Summary

ZEUS has measured hard photoproduction in a kinematic regime where the photon's structure has not yet been well-constrained. In both inclusive prompt- γ production and in dijet production the GRV photon parton densities are favoured over the GS96 parton densities. The data reveal fundamental phenomena of the theory

of QCD. A suppression of the resolved component of the photon with increasing photon virtuality has been observed and the effect of QCD dynamics on the angular distribution of two- and three-jet events has been studied. New photoproduction territory will shortly become accessible to the HERA experiments as we move into a regime of high luminosity HERA running.

References

- [1] ZEUS Collab., J. Breitweg et al., contribution 810 to *XXIX International Conference on High Energy Physics*, August 1998, Vancouver.
- [2] G. Marchesini et al., *Comp. Phys. Comm.* **67**, (1992) 465.
- [3] ZEUS Collab., J. Breitweg et al., contribution 812 to *XXIX International Conference on High Energy Physics*, August 1998, Vancouver.
- [4] ZEUS Collab., J. Breitweg et al., contribution 815 to *XXIX International Conference on High Energy Physics*, August 1998, Vancouver.
- [5] ZEUS Collab., J. Breitweg et al., contribution 816 to *XXIX International Conference on High Energy Physics*, August 1998, Vancouver.
- [6] ZEUS Collab., J. Breitweg et al., contribution 805 to *XXIX International Conference on High Energy Physics*, August 1998, Vancouver.
- [7] ZEUS Collab., J. Breitweg et al., contribution 800 to *XXIX International Conference on High Energy Physics*, August 1998, Vancouver.
- [8] S. D. Ellis, Z. Kunszt and D. E. Soper, *Phys. Rev. Lett.* **69**, (1992) 3615.
- [9] S. Catani, Yu.L. Dokshitzer, M. H. Seymour and B. R. Webber, *Nucl. Phys. B* **406**, (1993) 187.
- [10] S. D. Ellis and D. E. Soper, *Phys. Rev. D* **48**, (1993) 3160.
- [11] ZEUS Collab., M. Derrick et al., *Phys. Lett. B* **384**, (1996) 401.
- [12] H.-U. Bengtsson and T. Sjöstrand, *Comp. Phys. Comm.* **46**, (1987) 43.